

Enhancing heat transfer performance of automotive car radiator using camphor nanoparticles: experimental study with bibliometric analysis

Aditya Kolakoti¹, Muji Setiyo^{2,3*}, Dwi Novia Al Husaeni⁴ and Asep Bayu Dani Nandiyanto⁴

¹ Department of Mechanical Engineering, Raghu Engineering College, Visakhapatnam, **INDIA**


² Department of Mechanical Engineering, Universitas Muhammadiyah Magelang, Magelang, **INDONESIA**

³ Center of Energy for Society and Industry (CESI), Universitas Muhammadiyah Magelang, Magelang, **INDONESIA**

⁴ Department of Chemistry, Universitas Pendidikan Indonesia, Bandung, **INDONESIA**

* Corresponding Author: muji@unimma.ac.id

Received Aug 21st 2023; Revised Sep 25th 2023; Accepted Sep 29th 2023

 Cite this <https://doi.org/10.24036/teknomekanik.v6i2.25072>

Abstract: In this study, an attempt was made to investigate the heat transfer performance of a four-wheeler automotive radiator using a novel coolant system. To support this study, we also added bibliometric analysis to show the importance of this study. In the experiments, camphor nanoparticles (sizes of 511 nm) with various loadings (i.e. 2, 4, 6, and 8%) were mixed with deionized water (DW) to create a coolant. The experiments were conducted at different heat convection processes (i.e. 0.5, 1.45, and 3.7 m/s). The significant heat transfer performance parameters, such as Reynolds number (Re), Nusselt number (Nu), overall heat transfer coefficient (U), and heat transfer rate (Q), were examined. The Fourier Transform Infrared results revealed the presence of significant functional groups in the coolant system. camphor nanoparticles dispersed in DW were stable for more than 8 hours. At 70 °C, the novel coolant (2% camphor nanoparticles in DW) exhibits better Re, Nu, U, and Q than that using pure DW or other loadings of nanoparticles (e.g. 4, 6, and 8%). The high percentage of camphor nanoparticles in DW restricts the fluid flow, resulting in a drop in overall heat transfer performance. Finally, low-cost, easily available, and eco-friendly camphor nanoparticles (2%) are suggested as a better choice in lieu of high-cost metallic and non-metallic nanoparticles as an additive in the coolant system.

Keywords: Bibliometric; Camphor Nanoparticles; Coolant; Radiator; Thermal Conductivity; Heat Transfer Rate.

1. Introduction

Internal combustion (IC) engines are considered the most significant engines widely used in industrial, automotive, and agriculture applications. The work of an IC engine involves the conversion of chemical energy in hydro-carbon fuel to heat energy by compression and combustion. The compression and combustion increase the pressure and temperature inside the combustion chamber, which helps the connected piston to produce the desired output. The high pressure and temperatures are essential for IC engines to produce the desired results, but at the same time, they damage the engine components and produce toxic NO_x emissions [1]. It is always desirable to maintain low-temperature combustion [2]. Literature on thermodynamic analysis of various heat losses from an IC engine fueled with different fuels reveals that heat losses from the engine, especially the cooling losses, are also significant and contribute towards low engine performance [3]–[5]. Therefore, an effective way of removing the excess heat from the engine is to provide better cooling, and this can be achieved with the help of a heat exchanger called a radiator.

Radiators are often used in a wide variety of IC engines to remove unwanted heat from the system and maintain the engine in good condition. Therefore, improving the performance of a radiator has a positive impact on engine performance. Thus, the engine researchers focused on improving heat transfer performance in the radiator by modifying the design parameters like increasing the surface area, flow rate, and temperature gradient between the hot and cold fluids [6], [7]. These techniques have certain advantages as well as limitations. It is also evident from the literature [6] that refining the heat transfer performance in radiators by altering the radiator design, like increasing the surface area of fins, has already reached its limits. Now, the effective way to improve a radiator's performance is not to focus on the radiator design but to improve the thermal properties of the working fluids used in the radiators.

Ethylene glycol ($C_2O_6H_2$) and water (H_2O) are commonly used as a coolant in the radiator, but with the increase in compression ratios and number of engine cylinders, the traditional coolants have become insignificant in improving the radiator performance. Therefore, research on high thermal conductivity, high specific heat, environment-friendly and more available coolants for heat transfer applications are gaining wide attention [8], [9]. On the contrary, the advent of nanofluids [9] as a coolant in radiators improves performance. Ponangi, B. R *et al.* [10] examined the performance of a liquid-air automotive radiator using low-volume concentrations of carboxyl graphene, graphene oxide, and novel hybrid nanoparticles. The reported results reveal a significant improvement in the liquid air automotive radiator's performance in terms of effectiveness (232% improvement) and pressure drop (66% reduction). Furthermore, the functionalized graphene and hybrid nanoparticles offer great scope to improve the radiator's performance. Another study [11] used the Multiwalled Carbon Nanotube Nanoparticles (MWCNT) in a mixture of water and ethylene glycol at 50:50 volume ratios to test the heat transfer performance in an automotive radiator. The results proved that increasing the nanoparticle concentration improves the radiator's heat transfer performance. Furthermore, the authors observed a high aggregation and sedimentation of nanoparticles after the experimentation.

If considered at the nanoscale, the Van der Waals forces are observed to be weak, which may cause the aggregation of the nanoparticles. Gravity is also a fundamental cause for the nanoparticles to settle, and most of the nanoparticles currently in use are of metallic and metallic oxides having improved heat transfer properties [9]. Furthermore, the aggregation of nanoparticles is caused by high surface free energy, which forces the nanoparticles in the base liquids for fast settling [12]. Agglomeration or accumulation of nanoparticles leads to operational issues like clogging passages during transportation. Though metal base nanoparticles showed a significant improvement in the radiator performance due to enhanced properties of high thermal conductivity, the problems of accumulation and permanent deposition of nanoparticles are challenging [13]. Therefore, the preparation of nanofluids is one of the crucial stages for maintaining the degree of stability [12]. For this purpose, the addition of surfactants and ultrasonic or mechanical mixing is widely in use. Ilyas *et al.* [14], in their review article on the preparation, sedimentation, and agglomeration of nanofluids, showed two strategies for preparing stable nanofluids. Another study by Efemwenkikie *et al.* [15] used a bio-extract (Malay Apple) doped mono and hybrid nanofluids to investigate the heat transfer performance. The results showed that Malay apple extract significantly enhanced the heat transfer property in a light-duty down-flow radiator. From the start of milli-to micro-sized particles as an additive to the present day's use of nano-sized particles, there has been a drastic improvement in heat transfer properties with the application of different metals, non-metals, and biobased extracts as coolants in radiators. In this experimental investigation, an attempt is made to introduce a novel nanoscale particle that is readily available and possesses good coolant properties.

Unlike traditional coolants like Ethylene glycol, Propylene glycol, and different types of nanoparticles, this study proposed a novel nanoscale camphor powder mixed with deionized water as a coolant to examine the heat transfer property in an automotive car radiator. Camphor can be

found in the wood of the camphor tree (*Cinnamomum camphora*), which is a large evergreen tree in Asia. Camphor has a rich history of traditional usage, and it appears to be a white or transparent solid with a strong aromatic odor. The chemical formula of camphor is $C_{10}H_{16}O$, which is a terpenoid compound. Due to the structure, as shown in Figure 1, camphor exhibits excellent biological properties of antimicrobial, antiviral, and medicinal use [16]. Moreover, camphor is a biodegradable and eco-friendly material [17], which is a need-of-the-hour characteristic that other metallic nanoparticles do not have. Therefore, an attempt was made in this study to examine the heat transfer performance in a radiator using various loadings (i.e. 2, 4, 6, and 8%) of camphor nanoparticles mixed with deionized water and to evaluate the significant parameters like over-all heat transfer coefficient, heat transfer rate, Reynolds number, and Nusselt number. To support this experiment, we also added a bibliometric analysis to understand the importance of this study.

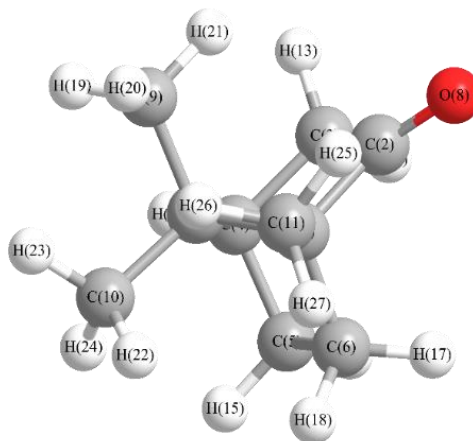


Figure 1: Schematic structure of camphor

2. Material dan methods

2.1 Preparation characterization and blending of camphor nanoparticles

The camphor used in this experimental investigation is obtained from Cipla Laboratories in Visakhapatnam, India. The obtained solid camphor is in sphere shaped pallets and appears in white, as shown in Figure 2(a), and the significant properties of camphor are highlighted in Table 1. The camphor is claimed to be purified to more than 99% and is utilized as-is. The sample is a powder when kept at room temperature. Because of the solid state, the KBr pellet procedure is used to prepare the samples for IR spectral analysis. The compound's spectrum is recorded using a "Perkin Elmer Spectrum Two FTIR-ATR spectrophotometer equipped with a diamond as the internal reflection element, and 100 scans at a resolution greater than 2 cm^{-1} " [18].

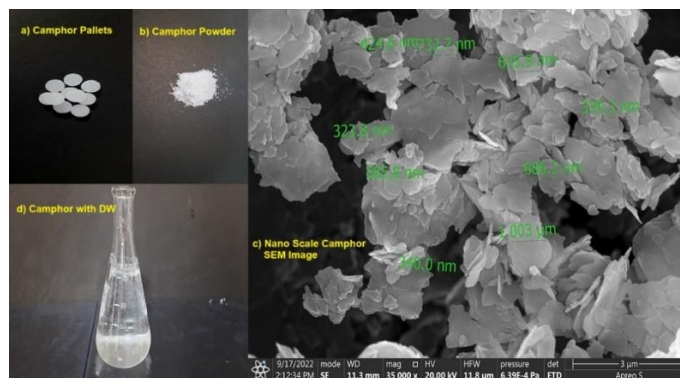


Figure 2: Preparation of camphor nano particles and blending

The conversion of camphor into nano-size particles is initiated with a grinding process; for this purpose, Kanchan Ganga grinding machine is utilized. The camphor pallets are grind into a fine powder, as shown in Figure 2(b), and the average size of the camphor nanoparticles are observed as 511 nm from SEM analysis as shown in Figure 2(c) and the camphor nanoparticles of varying percentages (2%, 4%, 6%, and 8% by volume) are mixed with deionized water (DW) as shown in Figure 2(d). To achieve a stable solution, a 750 watts high speed (21000 rpm) heavy-duty mixture machine (Kanchan Ganga) is utilized, and it is observed that the camphor nanoparticles are stable in deionized water for more than 8 hours. The significant properties of the coolant blends are presented in Table 2.

Table 1: Technical specifications of camphor

S.No	Property	Description
1	Chemical Formula	C ₁₀ H ₁₆ O
2	Color	White
3	Density (kg/m ³)	990
4	pH	6.8
5	Thermal Conductivity	0.7 W/mK
6	Specific heat	4107 J/kg-K
7	Flash Point (°C)	66
8	Molecular weight (g/mol)	173.42
9	Melting point range (°C)	180-185
10	Boiling point range (°C)	205-210

Table 2: Thermal properties of the coolant with different percentages of camphor nanoparticles

S.No	Property	2% C+DW	4% C+DW	6% C+DW	8% C+DW
1	Specific heat (J.kg ⁻¹ .K ⁻¹)	4108.5	3709.7	3203.6	3091.6
2	Viscosity (Poise)	0.0046	0.0041	0.0039	0.0042
3	Thermal Conductivity (W/mK)	0.685	0.676	0.662	0.642

2.2 Experimental setup

The experiments were conducted on the test rig presented in Figure 3. The test rig consisted of a heat exchanger called a radiator, which was obtained from Maruti Suzuki Genuine Parts located in Visakhapatnam, India. The radiator was widely used in four-wheeler Maruti Suzuki Automobiles, and its technical specifications are shown in Table 3. The radiator was fixed to the test bench, and both inlet and outlet from the radiator related to an insulated heat transfer pipe (PVC-Polyvinyl chloride), and the other ends of the pipes are connected to a stainless-steel reservoir tank of 15-litre capacity. An electrical-driven pump and fan are installed and connected to a power supply, as shown in the test rig. The fluid flow into the radiator can be adjusted manually with a control valve, as shown in Figure 3. Similarly, the airflow rate can also be adjusted with the help of an electrical regulator. The other significant instruments used in this study were Infrared thermometer (range of 50 to 550 °C, accuracy ±1.5 °C), digital temperature measuring thermocouples (range of -50 to 110 °C, accuracy ±1 °C), digital anemometer (range 0-30 m/s, threshold 0.1, accuracy ±5%), rotameter (range 2-60000 litre/hr, accuracy ±2% full-scale deflection) DC power supply unit, and an electrical heater (Bajaj 1500 Watt immersion type).

The experimentation was started with a trial run to check the connections and any leakages from the system. Once the verification had been completed, the experimentation of measuring the

radiator's performance with camphor particles was started at ambient conditions ($\pm 29^\circ\text{C}$). Initially, the tank was filled with 2% of stable camphor nanoparticles in DW and heated (up to 70°C) with the help of an electric heater. After achieving the desired temperature in the storage tank, the pump was put into action. The fluid flow rate into the system can be monitored with a rotameter and a control valve. For convective heat transfer, an electrically driven fan was connected near the radiator, and the rotation speed (rpm) of the fan can be adjusted with the help of a regulator. Similarly, the temperature drop in the system was recorded with the help of thermocouples fixed at different locations like the inlet, outlet, and on the wall of the radiator. At different air flow rates, the experiments were conducted for 2, 4, 6, and 8% of camphor nanoparticle loading in DW, and the experimentations were repeated thrice to lower the errors.

Table 3: Technical specifications of the automotive radiator

S.No	Specifications	Details
1	Number of tubes	36
2	Length of the tube	35.5 cm
3	Width of the tube	0.2 cm
4	Fin thickness	0.1 cm
5	Length of the Fin	2.5 cm
6	Width of the Fin	1.9 cm
7	Length \times Width \times Height of the Radiator	43 \times 37.5 \times 3.4 cm

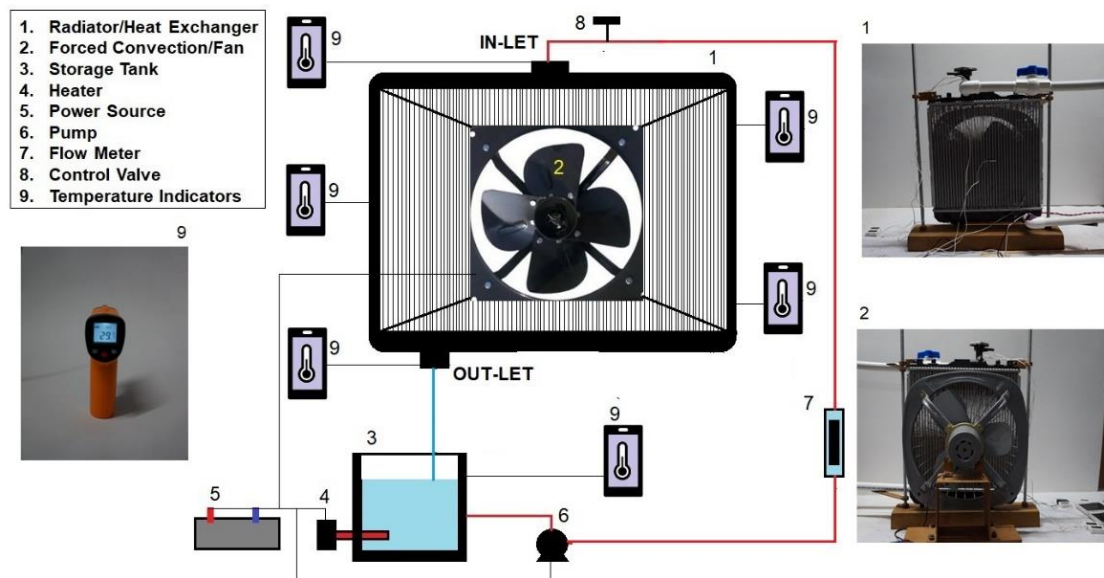


Figure 3: Schematic layout of the experimental setup

2.3 Mathematical heat transfer relations

The mathematical relations for computing the significant heat transfer performance parameters [8], [10], [11], [15] such as Reynolds number (Re), Nusselt number (Nu), Prandtl number (Pr), Overall heat transfer coefficient (U) and heat transfer rate (Q) from the radiator were discussed in the following Eqs. (1) - (20). The mathematical relation for the coolant side was formulated by Eqs. (1) to (3).

$$Re_c = \frac{\rho_c \times V_c \times D_h}{\mu_c} \quad (1)$$

where Re_c denotes the Reynolds number of the coolant and the density of the coolant is denoted by ρ_c . Similarly, the velocity of the coolant denoted by V_c , hydraulic diameter as D_h , and the viscosity of the coolants as μ_c .

$$Nu_c = 0.023 (Re_c)^{0.8} (Pr_c)^{0.4} \quad (2)$$

where Nu_c denotes the Nusselt number of the coolant and Pr_c as Prandtl number.

$$Pr_c = \frac{\mu_c \times CP_c}{K_c} \quad (3)$$

where CP_c and K_c represent the specific heat capacity and thermal conductivity of the coolant. Like the Equations (1) - (3), the correlations for the air side are as formulated by Eq. (4) to (7).

$$Re_a = \frac{\rho_a \times V_a \times W_{tube}}{\mu_a} \quad (4)$$

$$Nu_a = 0.664 (Re_a)^{0.5} (Pr_a)^{0.3} \quad (5)$$

The heat transfer coefficient for airside h_a and coolant side h_c are represented as:

$$h_a = \frac{Nu_a \times K_a}{W_{tube}} \quad (6)$$

$$h_c = \frac{Nu_c \times K_c}{D_h} \quad (7)$$

The characteristic length of the fin (L_c) is calculated with Eq. (8).

$$L_c = L_{fin} + \frac{H_{fin}}{2} \quad (8)$$

where L_{fin} represents the length of the fin and H_{fin} is the height of the fin. The single fin surface area is represented by Eq. (9).

$$A_f = 2W_{fin}L_c \quad (9)$$

where W_{fin} represents the width of the fin. The base surface area of the fin is calculated with Eq. (10).

$$A_b = (2L_{radiator}W_{tube}) - (H_{fin}W_{fin}n_{fin}) \quad (10)$$

where $L_{radiator}$ represents the length of the radiator, W_{tube} is the width of the radiator tube, and n_{fin} is the number of fins per tube top and bottom. The ratio of the total single tube surface area to the base surface area is calculated by Eqs. (11) and (12).

$$A_{fb} = n_{fin}A_f + A_b \quad (11)$$

$$m = \left(\frac{2h_A}{k_{radiator}H_{fin}} \right)^{0.5} \quad (12)$$

The total internal and external surface area of the radiator is calculated with the following Eqs. (13) and (14), where H_{tube} represents the height of the radiator tube, and n indicates the number of tubes.

$$A_{internal} = 2(W_{tube} + H_{tube})(nL_{radiator}) \quad (13)$$

$$A_{external} = nA_{fb} \quad (14)$$

The overall efficiency of the fin is calculated by Eq. (15).

$$\eta_0 = \frac{\tanh(mL_c)}{mL_c} \quad (15)$$

The overall heat transfer coefficient (W/K) of the radiator is calculated with Eq. (16).

$$\frac{1}{UA} = \frac{1}{(\eta_0 hA)_A} + \left(\frac{R_f}{\eta_0 A} + \frac{1}{\eta_0 hA} \right)_c \quad (16)$$

The heat transfer rate is calculated with Eq. (17).

$$Q = UA\Delta T \quad (17)$$

where ΔT represents the logarithmic mean temperature difference and can be represented by Eq. (18).

$$\Delta T = \frac{\Delta T_1 - \Delta T_2}{\ln\left(\frac{\Delta T_1}{\Delta T_2}\right)} \quad (18)$$

Finally, the temperature gradients (ΔT_1 and ΔT_2) of the radiator are calculated by Eqs. (19) and (20).

$$\Delta T_1 = Tc_{in} - Ta_{out} \quad (19)$$

$$\Delta T_2 = Ta_{in} - Tc_{out} \quad (20)$$

2.4 Uncertainty analysis

The experimental setup consists of nonlinear parameters that are changed according to space and time. Therefore, uncertainty analysis helps in quantifying the variability of output, which is caused due to variability in input. The uncertainty is carried out by the identification of errors in the measured parameters and measuring instruments like temperature and fluid flow rate. The uncertainties in different parameters are computed according to the uncertainty analysis described by Beckwith *et al.* [19], and their detailed calculations are presented in Appendix A. The obtained results of uncertainties are highlighted in Table 4.

Table 4 : Uncertainty of measured parameters

S.No	Parameter	Uncertainty (\pm %)
1	Temperature Sensor	0.0832
2	Hydraulic Diameter	0.625
3	Reynolds Number	0.1
4	Nusselt Number	0.1547
5	Heat Transfer Rate	0.0838

2.5 Chemical analysis

To support the analysis, Fourier Transform Infrared (FT-IR) was used. Detailed information regarding the analysis of FT-IR is explained in previous literature [20], [21].

2.6 Bibliometric analysis

To support the analysis, bibliometric analysis was carried out. In short, we used "Heat Transfer" OR "Automotive Car Radiators" OR "Nanoparticles" as the keywords. The article data used is article data indexed by Google Scholar in 2018 – 2023 and the Publish or Perish application. Detailed information for the bibliometric analysis is shown in previous studies [22], [23].

3. Results and discussion

3.1 Bibliometric analysis to view publication trends

Research trends regarding "Heat Transfer" OR "Automotive Car Radiators" OR "Nanoparticles" can be seen in Figure 4. This figure shows the importance of research on the effect of additional nanoparticles on the heat transfer phenomena, especially in car radiators, showing the excellent relationship between terms of these keywords.

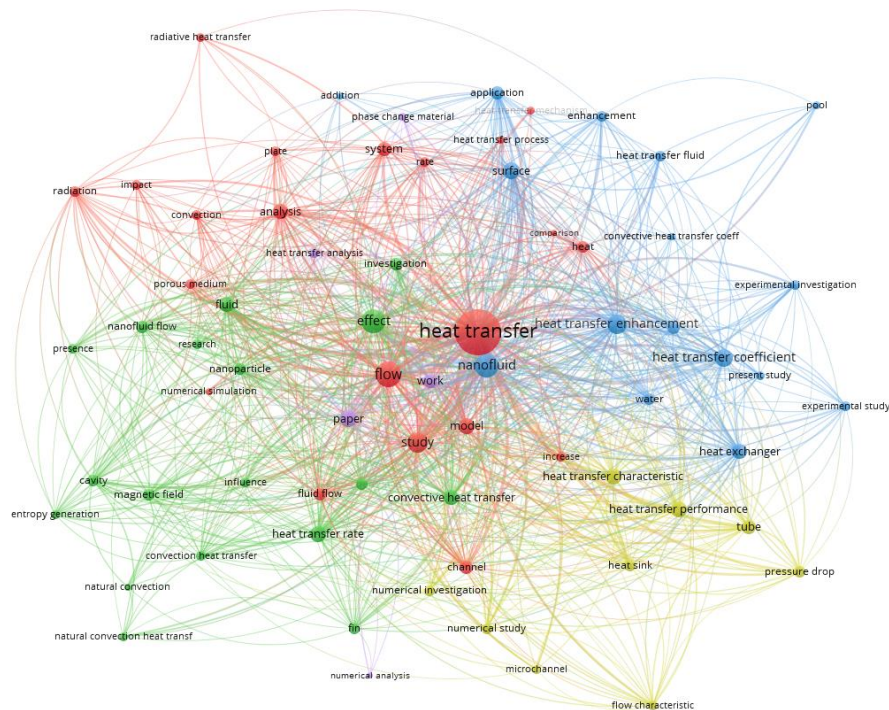


Figure 4: Network visualization based on keyword

3.2 FT-IR spectrum analysis of camphor

FT-IR is a practical means of examining chemical bonding in a substance in a non-destructive manner. Different bonds act distinctly to input radiation because of changes in their molecular stretchings and bending vibrations. Reactivity may be characterized by monitoring the IR radiation transmission percent and by comparing it with the existing chemical bond type and nature identifiers. Standard FT-IR analyses of camphor spectra suggest that the compound has a significant number of functional groups that could be categorized into distinct individual classes. Detailed information for the FT-IR analysis is shown in previous literature [20], [21]. The stretching groups of CH₂ can be recognized in "the FT-IR" of the camphor as wavenumber bands 2962, and 2874 cm⁻¹

¹ in the “Infrared Spectrum”. The wavenumber 1742 cm^{-1} is allotted to $\text{C}=\text{O}$ stretchings of the camphor. The wavenumber 1475 and 1448 cm^{-1} is imputed to the βCH_2 rocking and βCH_2 Scissoring of CH_2 in-plane bending modes of the camphor [24]. The CC stretching vibrational modes are identified in Camphor's infrared spectra as bands 1418 , and 1389 cm^{-1} . The one βCH_3 and one βCH mode of in-plane bending of the camphor were assigned to the wavenumber bands 1373 cm^{-1} , and 1324 cm^{-1} , severally. The ring bending mode is designated as a wavenumber of 1277 cm^{-1} in camphor's “infrared spectrum”, respectively [24].

“Infrared spectra” of Camphor have allowed the assignment of νCC ring modes in the 1195 and 1095 cm^{-1} wavenumber range. The CH_2 Twisting and βCH_2 Wagging modes of camphor appeared to produce the bands visible in “the Fourier transform infrared spectra” of the antiemetic medication. This band frequency was identified as 1046 and 1022 cm^{-1} , severally. The “infrared spectra” of the cooling agent exhibited a peak at 930 cm^{-1} , which is imputed to the “in-plane bending mode” of the Ring Trigonal deformation mode [24]. It is identified that the “ ωCH mode” of the camphor corresponds to the frequency 855 cm^{-1} . In “the infrared spectra” of the titular agent, the bending mode of βCCO was found to correspond to the frequency 751 cm^{-1} .

According to the result obtained, the frequency bands 651 cm^{-1} identified in “the infrared spectra” of Aprepitant are due to the drug's “Torsional Ring asymmetric deformation of the camphor. The 551 cm^{-1} wavenumber was thought to be the βCCN , βNCC modes. In “the infrared spectrum of the agent, the torsional mode” of τCCCO could be given the value of 520 cm^{-1} . Based on “the FT-IR spectrum” of camphor, the “out-of-plane bending mode ωCC ” could be linked to the wavenumber 475 cm^{-1} in “the IR spectrum”[20]. The “torsional bending modes” $\tau\text{Ring trid}$, $\tau\text{Ring asyd}$ of camphor have been imputed to “the frequency band” 451 cm^{-1} of the Camphor's FT-IR spectrum. From “the FT-IR spectra of the” camphor, as shown in Figure 5, it has been found that the torsion τCCCH is related to wavenumber 416 cm^{-1} [25]. Furthermore, the frequency corresponding to transmission and functional group assignment of camphor is present in the Appendix-B.

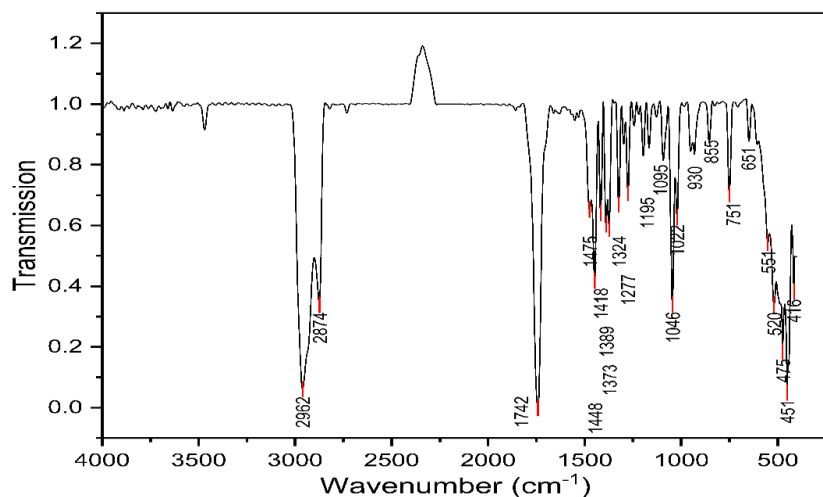


Figure 5: FT-IR spectrum of camphor with different functional groups

3.3 Analysis of reynolds number

The flow pattern or transportation property of a fluid in each system can be gauged with the Reynolds numbers (Re), and the Re helps determine whether the flow belongs to laminar, transient, or turbulent. In this experimental investigation, maximum Re is obtained below 1300; therefore, the flow is considered laminar. The variations of Re with respect to fluid velocity and

concentration of camphor in DW are shown in Figure 6. The maximum Re of 1240.93 is acclaimed for 2% of camphor nanoparticles in DW, followed by 1195.34 for pure DW. With the increase in camphor nanoparticles percentage in DW, there is a drop in Re witnessed. This is due to the accumulation of solid camphor nanoparticles in the flow channels that obstruct the coolant flow inside the radiator. Furthermore, the camphor possesses a density of 990 kg/m^3 and with the increase in camphor percentage in DW, the viscosity further improved and prevented the flow inside the radiator. The low Re represents the domination of viscous forces upon the inertial forces that help in maintaining a laminar flow pattern. The 2% of camphor nanoparticles in DW is recorded as the highest Re, which may be due to the presence of a low concentration of camphor amount, and the viscosity decreased with an increase in temperature. Similarly, a curve between the Nu and Re is drawn for varying percentages of camphor nanoparticles in DW, as shown in Figure 7. At a specific condition of Nu (value of 10.26) and Re (value of 1240), 2% of camphor nanoparticles in DW is recorded as the maximum. 8% of camphor nanoparticles in DW is recorded as the lowest at a specific condition of Nu (value of 4.13) and Re (value of 550). With the increase in the camphor nanoparticles percentage in DW, there is a drop in both the Nu and Re is witnessed, which is due to the agglomeration [11], [26].

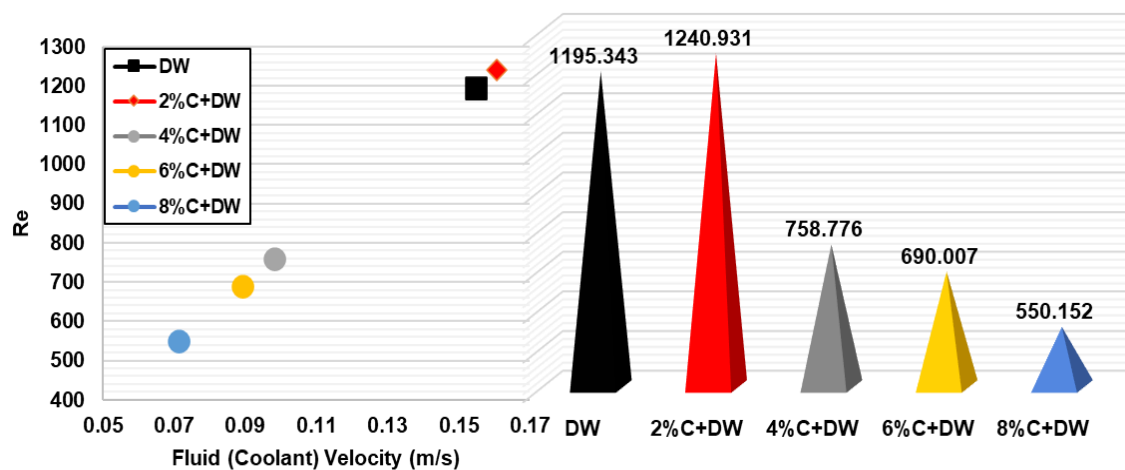


Figure 6: Variation of Re at different velocities and different coolants

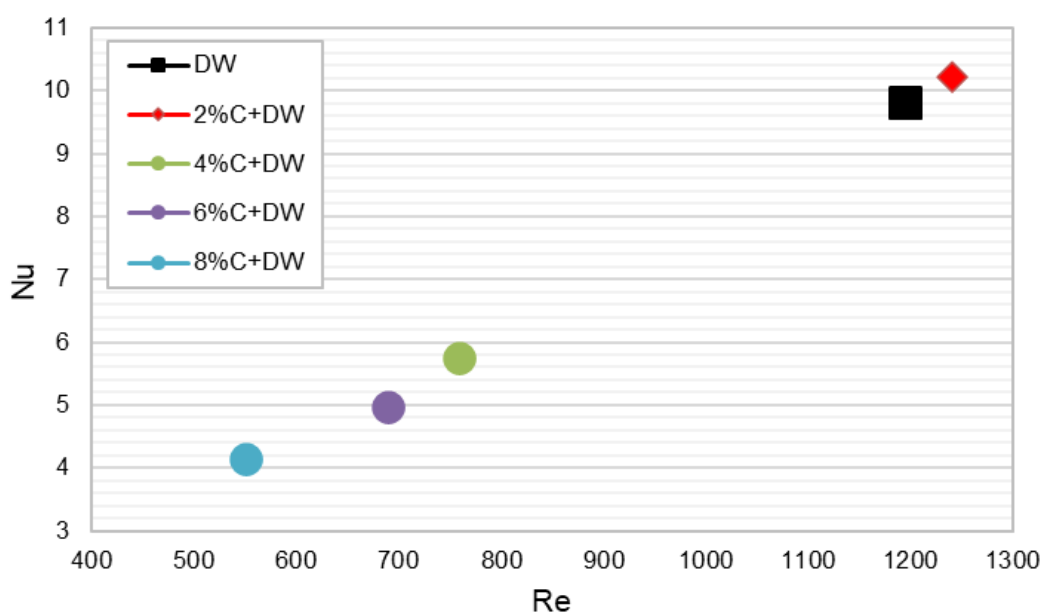


Figure 7: Variation of Nu with Re for different coolants

3.4 Analysis of nusselt number

The variations in Nusselt number (Nu) for deionized water (DW) and various percentages of camphor nanoparticles with DW are shown in Figure 8. It is evident that 2% of camphor nanoparticles in DW recorded as the highest Nu of 10.216, which is 4.29% higher than that using pure DW. The definition of Nu reveals that convection and conduction play a significant role in improving heat transfer in heat exchangers like radiators. These dimensionless parameters help in estimating the heat transfer between the moving fluid and a system. In this study, the moving fluid is various percentages of camphor nanoparticles with DW as a coolant. Compared to 8, 6, and 4% of camphor loadings as well as pure DW, the 2% of camphor in DW dominates the other coolant combinations due to a better Reynolds number and Prandtl number that helps improve the Nu. However, with the increase in the camphor percentage in DW, there is a downfall of Nu witnessed. This is due to the increase in micron size concentration restricting the volume flow of the coolant, and the same is observed in Figure 8 as the highest concentration of camphor, i.e., 8%, recorded as the lowest velocity rate. Furthermore, adding camphor nanoparticles in DW improves the viscosity of the coolant. Similar studies [27], [28] on radiators using different nanoparticles to enhance heat transfer performance reported similar results.

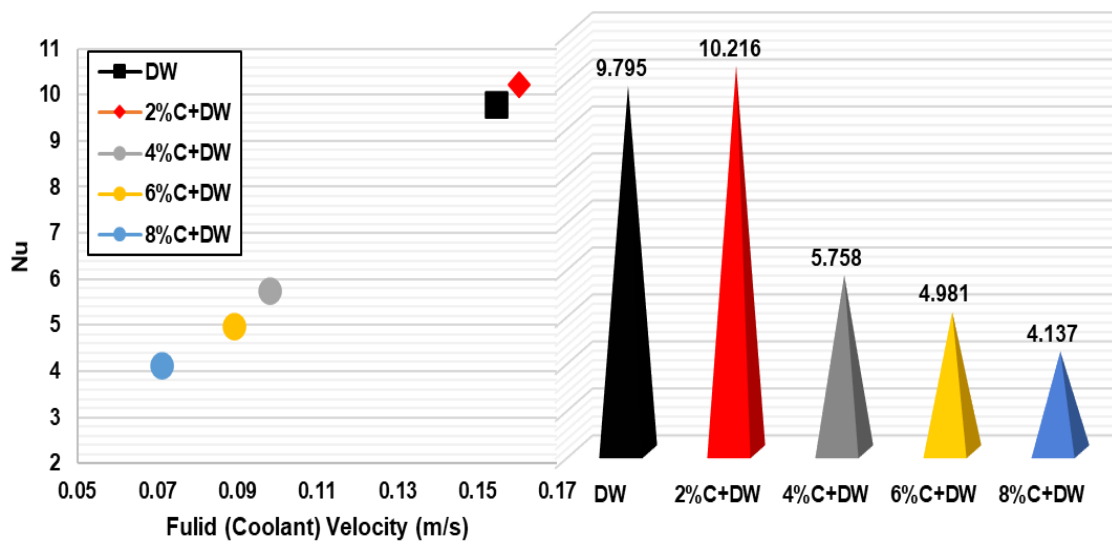


Figure 8: Variation of Nu at different velocities and different coolants

3.5 Analysis of heat transfer coefficient and heat transfer rate

In compact systems like radiators, the heat transfer rate is challenging to measure with individual heat transfer coefficients. However, measuring the heat transfer rate with the overall heat transfer coefficient is possible. Therefore, the overall heat transfer coefficient (U) and the heat transfer rate (Q) are computed based on Eqs (16) and (17), as discussed in section 2.3, and the variations are reported in Figure 9 and Figure 10.

Figure 9 presents the overall heat transfer coefficient (U) for tested coolants (2%, 4%, 6%, and 8% camphor nanoparticles in DW) at different fan speeds. It is observed that with the increase in air velocity, the U also increases. At the maximum velocity of 3.7 m/s, the U is recorded as 151.7 W/m²K for DW and 154.3 W/m²K for 2% of camphor nanoparticles in DW. Similarly, 142; 138.6; and 132.4 W/m²K are recorded for 4, 6, and 8% of camphor nanoparticles in DW, respectively. Compared to other percentages of camphor nanoparticles in DW, the 2% is observed as promising at all the fan speeds by achieving maximum overall heat transfer coefficient, and the increment is recorded as 1.71% higher than DW and 16.51% higher than 8% of camphor

nanoparticles in DW at 3.7 m/s. Similar trends are also observed at 0.5 and 1.45 m/s, where 2% of camphor nanoparticles in DW is recorded as the highest overall heat transfer coefficient. Similar to the overall heat transfer coefficient, the heat transfer rate (Q) variations are shown in Figure 9, which reported the domination of 2% of camphor nanoparticles in DW over other percentages. With the increase in fan velocity, the heat transfer rate from the heat exchanger is increased. The maximum heat transfer rate is achieved with the 2% of camphor nanoparticles in DW, recorded as 4287 W. The high heat transfer rate with the camphor nanoparticles is acclaimed for a better overall heat transfer coefficient. Furthermore, the fluid flow velocity for 2% of camphor nanoparticles in DW is higher than the other percentages, which helps achieve a better heat transfer rate as fluid velocity is one of the significant parameters that play a vital role in heat transfer, especially in forced convection [29]. With the implementation of high thermal conductivity camphor nanoparticles in DW, the heat transfer rate is improved. However, the higher concentrations regulate the flow pattern, thereby decreasing the overall performance of the radiator. Compared to DW, the 2% of camphor nanoparticles is recorded as 1.69, 1.18, and 0.82%, corresponding to a high heat transfer rate at 3.7; 1.45; and 0.5 m/s, respectively. It is evident that at low velocities, the heat transfer rate and convective heat transfer coefficient are observed to be low. Similar findings are reported with different nanoparticles tested in heat exchanges, and Table 5 compares present results with recent literature.

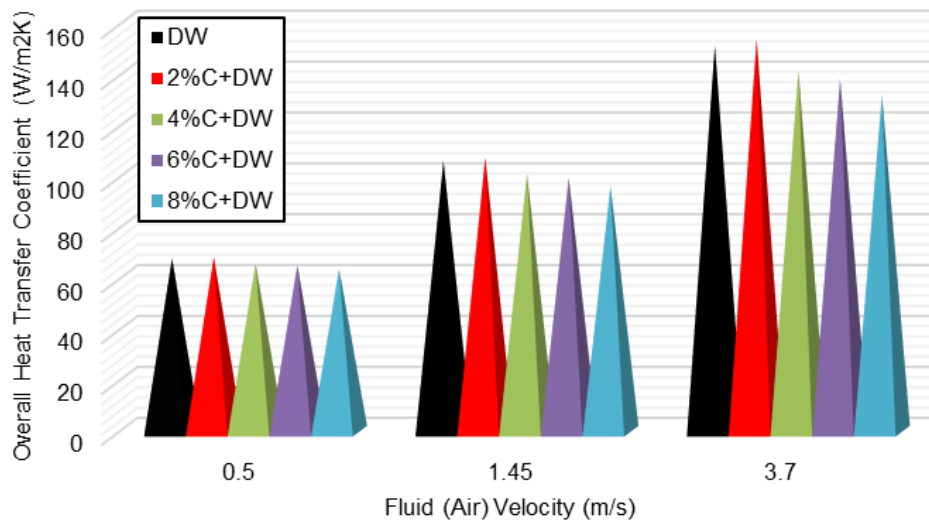


Figure 9: Variation of heat transfer coefficient with air velocity

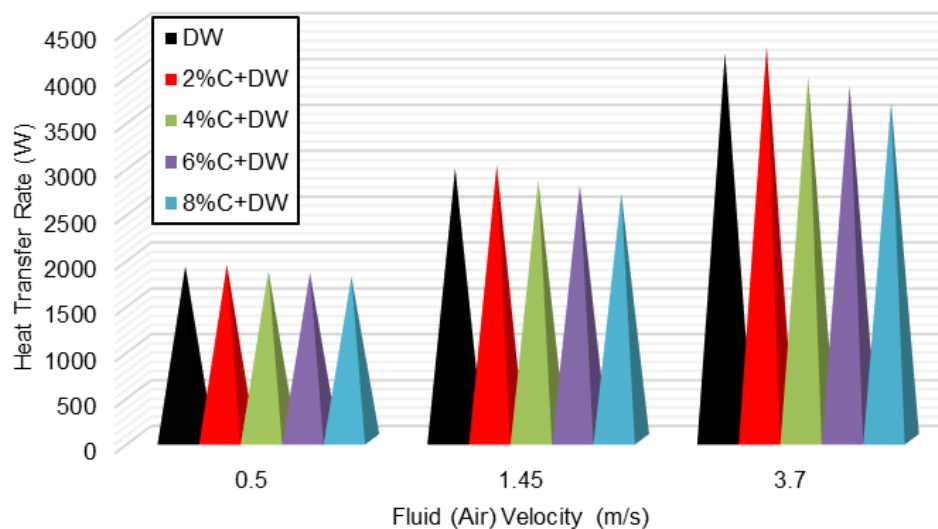


Figure 10: Variation of heat transfer rate with air velocity

Table 5: Comparison of recent findings in the literature with the present study

Type of Coolant and references	Findings	Present study
Al ₂ O ₃ and CuO Nanoparticles (0.05, 0.15, and 0.3%) concentration mixed with base fluid (50% water and 50% Ethylene Glycol) [30]. Pure water with suspended TiO ₂ and SiO ₂ nanopowders [31].	CuO nanofluids exhibit high heat transfer performance with better U (36384.41 W/m ² K), Q (28.45 W), and Nu 208.71. The results reveal that the SiO ₂ nanofluid shows a higher heat transfer improvement compared to the TiO ₂ nanofluid. It is also observed that Nu increased with volume flow rate and inlet temperature.	Thermal conductivity and flow rates play a significant role in improving the heat transfer performance in heat exchangers. It is also evident from the comparisons with the literature that high thermal conductivity nanoparticles improve the overall heat transfer performance. In this study, the heat transfer performance from the radiator is improved with the increase in flow rate and at maximum coolant flow, the better heat transfer performance is attributed to 2% of camphor in DW i.e., Re (1240.93), Nu (10.216), U (154.3 W/m ² K), Q (4287 W).
Fe ₂ O ₃ -TiO ₂ (50:50) is a hybrid nanoparticle suspended in a base fluid (water). The used nanoparticle volume concentrations are 0.005, 0.007, and 0.009% [32].	The 0.009 vol.% hybrid nanofluid shows a better heat transfer rate of 26.7% and Nu. The other hybrid nanofluids (0.005 and 0.007%) reported clogging, which diminished the stability and resulted in poor performance.	
The carboxyl-functionalized graphene nanoplatelets (CGnP) and TiO ₂ nanoparticles in a mixture of distilled water and ethylene glycol as base coolant [33].	The CGnP-TiO ₂ (70:30) with 0.1 wt% concentration mixed into the base coolant improves the Nu (4.94%), U (35.87%), and effectiveness (20.48%) of the radiator.	

4. Conclusion

This experimental investigation aims to enhance the heat transfer efficiency of a radiator used in four-wheeled automobiles. For this purpose, readily available and cost-effective camphor is utilized. Camphor nanoparticles are blended in varying proportions (2%, 4%, 6%, and 8%) with deionized water, and experiments are conducted under different fluid flow conditions. The outcomes of these experiments lead to the following conclusions.

1. The camphor nanoparticles in deionized water exhibit better coolant properties, and the camphor nanoparticles appear to be stable for more than 8 hours by physical observation.
2. The FTIR spectrum of camphor nanoparticles reveals the presence of functional group elements, which are significant in improving the heat transfer performance as a coolant.
3. The transportation property of the coolants is recorded below 1300. Therefore, the flow is considered laminar.
4. The maximum Reynolds number (1240.93) is recorded for 2% camphor nanoparticles in deionized water and the lowest for 8%. With the increase in camphor nanoparticles percentage, the Reynolds number decreases. On the other hand, the Reynolds number increased with the coolant velocity.

5. The Nusselt number increased with coolant velocity and decreased with increasing camphor percentages in deionized water. Compared to neat deionized water, 4%, 6%, and 8%, the 2% camphor nanoparticles were recorded as a high Nusselt number.
6. Similarly, the highest overall heat transfer coefficient of $154.3 \text{ W/m}^2\text{K}$ and heat transfer rate of 4287 W is recorded for 2% camphor nanoparticles in deionized water.

Currently, nanoparticles obtained from different metals and non-metals are widely in use for improving the performance of heat exchangers like radiators. However, these nanoparticles are costly and not biodegradable. Therefore, renewable, low-cost, and biodegradable nanoparticles are the need of the hour. In this study, camphor nanoparticles show an improvement in the performance of the radiator, and it is concluded that 2% camphor nanoparticles in deionized water are the better choice as a radiator coolant.

Author contribution

Aditya Kolakoti: conceptualization, conceived and designed the experiments, performed the experiments, analyzed and interpreted the data, wrote the original and revised paper; Muji Setiyo: analyzed and interpreted the data, data visualization, wrote the original and revised paper; Dwi Novia Al Husaeni: analyzed and interpreted the data, data validation, wrote the revised paper; Asep Bayu Dani Nandiyanto: analyzed and interpreted the data, data validation, wrote the original and revised paper.

Funding statement

This article is one of the outputs of collaborative research between Raghu Engineering College, India; Universitas Muhammadiyah Magelang, Indonesia; and Universitas Pendidikan Indonesia, Indonesia.

Acknowledgements

The authors would like to thank the laboratory technicians and english editors.

Competing interest

The authors declare no competing interest.

References

- [1] A. Kolakoti and B. V. A. Rao, "Performance and emission analysis of a naturally aspirated and supercharged IDI diesel engine using palm methyl ester," *Biofuels*, vol. 11, no. 4, pp. 479–490, May 2020, <https://doi.org/10.1080/17597269.2017.1374770>
- [2] M. Krishnamoorthi, R. Malayalamurthi, Z. He, and S. Kandasamy, "A review on low temperature combustion engines: Performance, combustion and emission characteristics," *Renewable and Sustainable Energy Reviews*, vol. 116, p. 109404, 2019, <https://doi.org/10.1016/j.rser.2019.109404>
- [3] M. Setiyo, D. Yuvenda, and O. D. Samuel, "The Concise Latest Report on the Advantages and Disadvantages of Pure Biodiesel (B100) on Engine Performance: Literature Review and Bibliometric Analysis," *Indonesian Journal of Science and Technology*, vol. 6, no. 3, pp. 469–490, 2021, <https://doi.org/10.17509/ijost.v6i3.38430>
- [4] A. Kolakoti, "Exergetic performance, combustion and emissions studies in a CI engine fueled with Al_2O_3 nano additive in a mixture of two different biodiesel and diesel blends,"

- Australian Journal of Mechanical Engineering*, pp. 1–16, 2022, <https://doi.org/10.1080/14484846.2022.2122174>
- [5] A. Kolakoti, A. V. Kumar, R. Metta, M. Setiyo, and M. L. Rochman, “Experimental studies on in-cylinder combustion, exergy performance, and exhaust emission in a Compression Ignition engine fuelled with neat biodiesels,” *Indonesian Journal of Science and Technology*, vol. 7, no. 2, pp. 219–236, 2022, <https://doi.org/10.17509/ijost.v7i2.49680>
- [6] A. Gheibi and A. R. Rahmati, “An experimental and numerical investigation on thermal performance of a new modified baseboard radiator,” *Applied Thermal Engineering*, vol. 163, p. 114324, 2019, <https://doi.org/10.1016/j.applthermaleng.2019.114324>
- [7] D. G. Charyulu, G. Singh, and J. K. Sharma, “Performance evaluation of a radiator in a diesel engine—a case study,” *Applied Thermal Engineering*, vol. 19, no. 6, pp. 625–639, 1999, [https://doi.org/10.1016/S1359-4311\(98\)00064-7](https://doi.org/10.1016/S1359-4311(98)00064-7)
- [8] K. Y. Leong, R. Saidur, S. N. Kazi, and A. H. Mamun, “Performance investigation of an automotive car radiator operated with nanofluid-based coolants (nanofluid as a coolant in a radiator),” *Applied Thermal Engineering*, vol. 30, no. 17, pp. 2685–2692, 2010, <https://doi.org/10.1016/j.applthermaleng.2010.07.019>
- [9] F. Abbas *et al.*, “Nanofluid: Potential evaluation in automotive radiator,” *Journal of Molecular Liquids*, vol. 297, p. 112014, 2020, <https://doi.org/10.1016/j.molliq.2019.112014>
- [10] B. R. Ponangi, V. Krishna, and K. N. Seetharamu, “Performance of compact heat exchanger in the presence of novel hybrid graphene nanofluids,” *International Journal of Thermal Sciences*, vol. 165, p. 106925, 2021, <https://doi.org/10.1016/j.ijthermalsci.2021.106925>
- [11] E. M. Cardenas Contreras and E. P. Bandarra Filho, “Heat transfer performance of an automotive radiator with MWCNT nanofluid cooling in a high operating temperature range,” *Applied Thermal Engineering*, vol. 207, p. 118149, 2022, <https://doi.org/10.1016/j.applthermaleng.2022.118149>
- [12] J. Patel, A. Soni, D. P. Barai, and B. A. Bhanvase, “A minireview on nanofluids for automotive applications: Current status and future perspectives,” *Applied Thermal Engineering*, vol. 219, p. 119428, 2023, <https://doi.org/10.1016/j.applthermaleng.2022.119428>
- [13] K. M. Jadeja, R. Bumataria, and N. Chavda, “Nanofluid as a coolant in internal combustion engine – a review,” *International Journal of Ambient Energy*, vol. 44, no. 1, pp. 363–380, Dec. 2023, <https://doi.org/10.1080/01430750.2022.2127891>
- [14] S. U. Ilyas, R. Pendyala, and N. Marneni, “Preparation, sedimentation, and agglomeration of nanofluids,” *Chemical Engineering & Technology*, vol. 37, no. 12, pp. 2011–2021, 2014, <https://doi.org/10.1002/ceat.201400268>
- [15] K. U. Efemwenkikie *et al.*, “Experimental investigation of heat transfer performance of novel bio-extract doped mono and hybrid nanofluids in a radiator,” *Case Studies in Thermal Engineering*, vol. 28, p. 101494, 2021, <https://doi.org/10.1016/j.csite.2021.101494>
- [16] F. J. Hammerschmidt, A. M. Clark, F. M. Soliman, E. S. El-Kashoury, M. M. Abd el-Kawy, and A. M. El-Fishawy, “Chemical composition and antimicrobial activity of essential oils of *Jasonia candicans* and *J. montana.*,” *Planta medica*, vol. 59, no. 1, pp. 68–70, Feb. 1993, <https://doi.org/10.1055/s-2006-959607>
- [17] R. Croteau and F. Karp, “Biosynthesis of monoterpenes: Hydrolysis of bornyl pyrophosphate, an essential step in camphor biosynthesis, and hydrolysis of geranyl pyrophosphate, the acyclic precursor of camphor, by enzymes from sage (*Salvia officinalis*),” *Archives of Biochemistry and Biophysics*, vol. 198, no. 2, pp. 523–532, 1979, [https://doi.org/10.1016/0003-9861\(79\)90527-7](https://doi.org/10.1016/0003-9861(79)90527-7)
- [18] I. Barra, L. Khiari, S. M. Haefele, R. Sakrabani, and F. Kebede, “Optimizing setup of scan number in FTIR spectroscopy using the moment distance index and PLS regression: application to soil spectroscopy,” *Scientific Reports*, vol. 11, no. 1, p. 13358, 2021, <https://doi.org/10.1038/s41598-021-92858-w>

- [19] T. G. Beckwith, N. L. Buck, and R. D. Marangoni, *Mechanical measurements*, vol. 5. Addison-Wesley New York, 1982.
- [20] A. B. D. Nandiyanto, R. Oktiani, and R. Ragadhita, "How to read and interpret FTIR spectroscopy of organic material," *Indonesian Journal of Science and Technology*, vol. 4, no. 1, pp. 97–118, 2019, <https://doi.org/10.17509/ijost.v4i1.15806>
- [21] A. B. D. Nandiyanto, R. Ragadhita, and M. Fiandini, "Interpretation of Fourier transform infrared spectra (FTIR): A practical approach in the polymer/plastic thermal decomposition," *Indonesian Journal of Science and Technology*, vol. 8, no. 1, pp. 113–126, 2023, <https://doi.org/10.17509/ijost.v8i1.53297>
- [22] D. F. Al Husaeni and A. B. D. Nandiyanto, "Bibliometric Using Vosviewer with Publish or Perish (using Google Scholar data): From Step-by-step Processing for Users to the Practical Examples in the Analysis of Digital Learning Articles in Pre and Post Covid-19 Pandemic," *ASEAN Journal of Science and Engineering*, vol. 2, no. 1, pp. 19–46, 2022, <https://doi.org/10.17509/ajse.v2i1.37368>
- [23] N. N. Azizah, R. Maryanti, and A. B. D. Nandiyanto, "How to search and manage references with a specific referencing style using google scholar: From step-by-step processing for users to the practical examples in the referencing education," *Indonesian Journal of Multidisciplinary Research*, vol. 1, no. 2, pp. 267–294, 2021, <https://doi.org/10.17509/ijomr.v1i2.37694>
- [24] P. Venkata Ramana, Y. Rama Krishna, and K. Chandra Mouli, "Experimental (FT-IR, UV-Vis) spectroscopic analysis and molecular docking investigations of anti-cancer drugs Alkeran and Bicalutamide," *Journal of Molecular Structure*, vol. 1270, p. 133984, 2022, <https://doi.org/10.1016/j.molstruc.2022.133984>
- [25] T. R. Sertbakan, "Structure, Spectroscopic and Quantum Chemical Investigations of 4-Amino-2-Methyl-8-(Trifluoromethyl)Quinoline," *Celal Bayar Üniversitesi Fen Bilimleri Dergisi*, vol. 13, no. 4, pp. 851–861, 2017, <https://doi.org/10.18466/cbayarfb.339858>
- [26] A. R. I. Ali and B. Salam, "A review on nanofluid: preparation, stability, thermophysical properties, heat transfer characteristics and application," *SN Applied Sciences*, vol. 2, no. 10, p. 1636, 2020, <https://doi.org/10.1007/s42452-020-03427-1>
- [27] N. S. Naveen and P. S. Kishore, "Experimental investigation on heat transfer parameters of an automotive car radiator using graphene/water-ethylene glycol coolant," *Journal of Dispersion Science and Technology*, vol. 43, no. 3, pp. 1–13, Mar. 2022, <https://doi.org/10.1080/01932691.2020.1840999>
- [28] S. Z. Heris, M. Shokrgozar, S. Poorpharhang, M. Shanbedi, and S. H. Noie, "Experimental Study of Heat Transfer of a Car Radiator with CuO/Ethylene Glycol-Water as a Coolant," *Journal of Dispersion Science and Technology*, vol. 35, no. 5, pp. 677–684, May 2014, <https://doi.org/10.1080/01932691.2013.805301>
- [29] A. M. Hussein, K. V Sharma, R. A. Bakar, and K. Kadrigama, "A review of forced convection heat transfer enhancement and hydrodynamic characteristics of a nanofluid," *Renewable and Sustainable Energy Reviews*, vol. 29, pp. 734–743, 2014, <https://doi.org/10.1016/j.rser.2013.08.014>
- [30] A. S. Tijani and A. S. bin Sudirman, "Thermos-physical properties and heat transfer characteristics of water/anti-freezing and Al₂O₃/CuO based nanofluid as a coolant for car radiator," *International Journal of Heat and Mass Transfer*, vol. 118, pp. 48–57, 2018, <https://doi.org/10.1016/j.ijheatmasstransfer.2017.10.083>
- [31] A. M. Hussein, R. A. Bakar, K. Kadrigama, and K. V Sharma, "Heat transfer enhancement using nanofluids in an automotive cooling system," *International Communications in Heat and Mass Transfer*, vol. 53, pp. 195–202, 2014, <https://doi.org/10.1016/j.icheatmasstransfer.2014.01.003>
- [32] F. Abbas *et al.*, "Towards convective heat transfer optimization in aluminum tube automotive radiators: Potential assessment of novel Fe₂O₃-TiO₂/water hybrid nanofluid," *Journal of the Taiwan Institute of Chemical Engineers*, vol. 124, pp. 424–436, 2021, <https://doi.org/10.1016/j.jtice.2021.02.002>

[33] H. W. Xian, N. A. C. Sidik, and R. Saidur, “Hybrid nanocoolant for enhanced heat transfer performance in vehicle cooling system,” *International Communications in Heat and Mass Transfer*, vol. 133, p. 105922, 2022, <https://doi.org/10.1016/j.icheatmasstransfer.2022.105922>

NOMENCLATURE

V_c	Velocity of the coolant in tubes	[m/s]
D_h	Hydraulic diameter	[m]
Cp_c	Specific heat of the coolant	[kJ/(kg · K)]
k_c	Thermal conductivity of the coolant	[W/(kg · K)]
h_c	Coolant convective heat transfer coefficient	[kJ/(m ² · K)]
V_a	Velocity of the air	[m/s]
W_{tube}	Width of the radiator tube	[m]
k_a	Thermal conductivity of the air	[W/(kg · K)]
h_a	Air convective heat transfer coefficient	[kJ/(m ² · K)]
L_c	Corrected fin length	[m]
L_{fin}	Length of the fin	[m]
A_f	Single fin surface Area	[m ²]
W_{fin}	Width of the fin	[m]
A_b	Base surface area of fin	[m ²]
$L_{radiatc}$	Length of the radiator	[m]
H_{tube}	Height of the radiator tube	[m]
ρ_c	Density of the coolant	[kg / m ³]
μ_a	Viscosity of the air	(N – s) / m ²
ρ_a	Density of the air	[kg / m ³]
μ_c	Viscosity of the coolant	(N – s) / m ²
n_{fin}	Number of the fins per tube top and bottom	
Nu_a	Nusselt number of the air	
Pr_a	Prandtl number of the air	
Re_a	Reynolds number of the air	
Re_c	Reynolds number of the coolant	
Nu_c	Nusselt number of the coolant	
Pr_c	Prandtl number of the coolant	

ABBREVIATION

C	Camphor
DW	Deionized water
FT-IR	Fourier transform infrared
IC	Internal combustion
IR	Infrared radiation
MWCNT	Multiwalled carbon nanotube nanoparticles.
Nu	Nusselt number
Nm	Nanometer
Q	Heat transfer rate
Re	Reynolds number
U	Overall heat transfer coefficient

Appendix-A

Uncertainty Calculations

The following steps are followed for the systematic error analysis to estimate the errors related to experimental analysis, such as Reynolds number, heat flux, overall heat transfer coefficient, and Nusselt number. Table A.1 lists the uncertainty in the values calculated using various equipment.

Table A.1 Uncertainties of instruments and properties

S.No	Instrument	Range	Variable measured	Least division in measuring instrument	Min. and max. values in experiment	Uncertainty (%)
1	Temperature sensor 1	-50 – 550 °C	Inlet fluid temperature	0.1 °C	48.7 – 71.4 °C	0.0832
2	Temperature sensor 2	-50 – 550 °C	Exit fluid temperature	0.1 °C	48.7 – 71.4 °C	0.0832
3	Temperature sensor 3	-50 – 550 °C	Surface temperature	0.1 °C	48.7 – 71.4 °C	0.0832
4	Rotameter	1 - 10000	Fluid flow	1 LPH	1 – 15L	0.01
5	Fan anemometer	0 – 30 m/s	Velocity of air	0.1 m/s	0.5 – 3.7 m/s	0.333
6	Properties	-	Thermal conductivity, density, specific heat, viscosity	-	-	0.1

Reynolds number (Re)

$$Re = \frac{4\dot{m}}{\pi D\mu}, \quad \frac{U_{Re}}{Re} = \sqrt{\left(\frac{U_{\dot{m}}}{\dot{m}}\right)^2 + \left(-\frac{U_{\mu}}{\mu}\right)^2} = \sqrt{(0.01)^2 + (-0.1)^2} = 0.1\% \quad (A.1)$$

Heat transfer rate (Q)

$$Q = \dot{m}c_p(T_i - T_o),$$

$$\frac{U_Q}{Q} = \sqrt{\left(\frac{U_{\dot{m}}}{\dot{m}}\right)^2 + \left(\frac{U_{(T_i - T_o)}}{T_i - T_o}\right)^2} = \sqrt{(0.01)^2 + (0.0832)^2} = 0.0838\% \quad (A.2)$$

Overall heat transfer coefficient (U)

$$U = \frac{Q}{A(\Delta T)}, \quad \frac{U_U}{U} = \sqrt{\left(\frac{U_Q}{Q}\right)^2 + \left(-\frac{U_{\Delta T}}{\Delta T}\right)^2} = \sqrt{(0.0838)^2 + (0.0832)^2} = 0.1181\% \quad (A.3)$$

Nusselt number (Nu)

$$Nu = \frac{hD}{k}, \quad \frac{U_{Nu}}{Nu} = \sqrt{\left(\frac{U_h}{h}\right)^2 + \left(-\frac{U_k}{k}\right)^2} = \sqrt{(0.1181)^2 + (0.1)^2} = 0.1547\% \quad (\text{A.4})$$

Hydraulic diameter (D_h)

$$Dp = \frac{4A}{P}, \quad \frac{U_{Dp}}{Dp} = \sqrt{\left(\frac{U_l}{l}\right)^2} = \sqrt{(0.625)^2} = 0.6255\% \quad (\text{A.5})$$

Appendix-B

FT-IR Analysis Data

Table B.1 Frequency corresponding transmission and functional group assignment of camphor

S.No	Wavenumber (cm ⁻¹)	Transmission (%)	Functional group
1	2962	0.93453	νCH
2	2874	0.65642	νCH ₂ meIn
3	1742	0.99645	νC=O
4	1475	0.34305	βCH ₂ T rocking
5	1448	0.57656	βCH ₂ Scissoring
6	1418	0.35425	νCC
7	1389	0.39038	νCC
8	1373	0.40547	βCH ₃
9	1324	0.32518	βCH
10	1277	0.28849	Ring bending
11	1195	0.16719	νCC ring
12	1095	0.18117	νCC ring
13	1046	0.6553	βCH ₂ Twisting
14	1022	0.36824	βCH ₂ Wagging
15	930	0.16496	Ring trid
16	855	0.12326	ωCH
17	751	0.29198	βCCO
18	651	0.11691	τ Ring asym d
19	551	0.45238	βCCN, βNCC
20	520	0.65681	τCCCO
21	475	0.81101	ωCC
22	451	0.94534	τRing trid, τRing asyd
23	416	0.61217	τCCCH

“**ν**: Stretching, **β**: In-plane bending, **ω**: Out-of-plane bending, **τ**: Torsion, **meIn**: Methylene, **ss**: symmetric stretching, **is**: in-plane stretching, **os**: out-of-plane stretching, **ir**: in-plane rocking **or**: Out-plane rocking, **ib**: in-plane bending, **ob**: Out-of-plane bending **d**: deformation **sym d**: Symmetric deformation, **asym d**: asymmetric deformation”.